CrystEngComm

PAPER

View Article Online
View Journal | View Issue

Cite this: *CrystEngComm*, 2016, **18**, 7021

'Frustrated' hydrogen bond mediated amphiphile self-assembly – a solid state study†

Laura R. Blackholly,[a] Helena J. Shepherd[b] and Jennifer R. Hiscock*[b]

Received 4th July 2016,
Accepted 24th August 2016

DOI: 10.1039/c6ce01493c

www.rsc.org/crystengcomm

Herein, we present the synthesis of ten structurally related 'frustrated' amphiphiles, from which were obtained eleven single crystal X-ray structures, allowing observation of the hydrogen bonding modes present in the solid state. We previously reported the synthesis of a novel amphiphilic salt which contains both hydrogen bond donating (HBD) and hydrogen bond accepting (HBA) functionalities. This amphiphilic salt was shown to self-associate in the solution state, aided by the formation of hydrogen bonds. The exact nature of the hydrogen bonding modes involved in this self-association process remains unclear due to the combination of HBD and HBA groups present in the amphiphile structure. This results in a 'frustrated' system with access to a variety of possible hydrogen bonding modes.

Introduction

Supramolecular interactions play a vital role in amphiphile self-assembly in the solution state, with hydrogen bonding, π–π stacking, electrostatics and charge transfer all known to drive molecular self-association and any resultant nanostructure.[1,2] In recent times supramolecular principles have been effectively utilised in the design of novel amphiphiles, giving rise to a new generation of bespoke self-associated nanostructures.[2–6] This has included work by Zhao and co-workers who have shown that low molecular weight, supramolecular-inspired amphiphiles are able to produce self-associated, hydrogen bonded nanocarriers with potential uses as novel drug or gene delivery systems.[7] Work such as this highlights the need to extend our fundamental knowledge of hydrogen bonded network formation within self-associated systems. This will further direct the fields of surfactant, formulation and materials science with direct implications for the detergent, cosmetic and pharmaceutical industries. Limited examples in this area include those by Oda and co-workers,[8] Bong and co-workers[9] and most recently our own work.[10]

The properties of anion-spacer-urea based amphiphiles have been studied extensively by Faustino and co-workers in the solution state.[11–14] Examples from this family of compounds have been shown to exhibit similar critical micelle concentrations to that of sodium dodecanoate. This is attributed to the hydrogen bonding properties of the urea functionality.[15] Our prior solution state work has centred on the *in situ* hydrogen bonding mode manipulation of the self-associated sulfonate-urea amphiphile, shown in Fig. 1. This type of sulfonate-urea based amphiphile contains two possible hydrogen bond acceptor (HBA) sites, the urea oxygen and sulfonate functionalities. However there is only one hydrogen bond donating (HBD) urea group. This results in a 'frustrated' system which can adopt a number of possible hydrogen bonding modes, as shown in Scheme 1. The modification of the different self-associated modes present was achieved through the addition of competitive HBD and HBA species. However, gaining insight into the exact nature of the hydrogen bonding modes present under specific conditions is no trivial task.[10]

In order to gain further knowledge as to how the hydrogen bonding modes adopted by this class of amphiphilic salt maybe altered by the chemical composition of the amphiphile, a total of ten related salts (**1–10**, Table 1) have now been synthesised. The R and X groups of **1–10** have been altered in a stepwise fashion to modify the acidity of the HBD

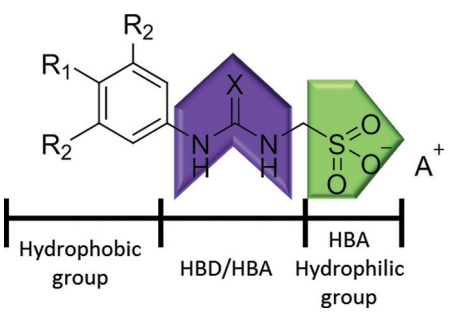

Fig. 1 General structure of the sulfonate-urea amphiphilic salts.

[a] *School of Biosciences, University of Kent, Park Wood Road, Canterbury, Kent, CT2 7NH, UK*
[b] *School of Physical Sciences, University of Kent, Park Wood Road, Canterbury, Kent, CT2 7NH, UK. E-mail: J.R.Hiscock@Kent.ac.uk; Tel: +44 (0)1227 823043*

† Electronic supplementary information (ESI) available: This includes experimental details and NMR and crystallography data. CCDC 1489604–1489612. For ESI and crystallographic data in CIF or other electronic format see DOI: 10.1039/c6ce01493c

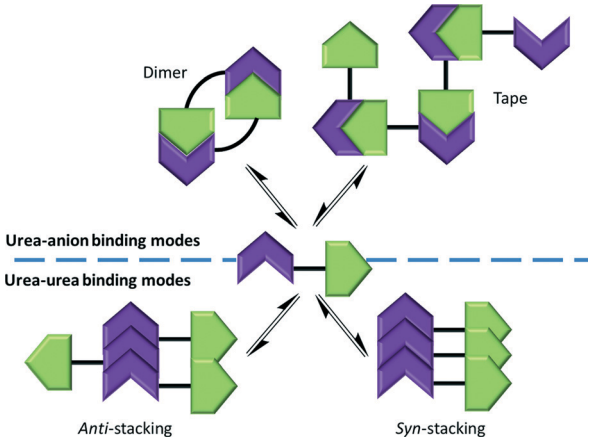

Scheme 1 Possible self-associated hydrogen bonded modes for this class of amphiphilic salt.

Table 1 Substituents of the general amphiphilic salt structure given in Fig. 1, giving rise to compounds **1–10**

Salt	R_1	R_2	X	A^+
1	OMe	H	O	TBA
2	H	H	O	TBA
3[a]	NO_2	H	O	TBA
4[a]	CF_3	H	O	TBA
5	CF_3	H	S	TBA
6	H	CF_3	O	TBA
7	H	CF_3	S	TBA
8[a]	CF_3	H	O	K
9	CF_3	H	O	Na
10	CF_3	H	O	Pyridinium

[a] Reported previously.[10] TBA = tetrabutylammonium.

NH groups while the substitution of different counter cations explore ion pair effects. Eleven different single crystal X-ray structures have been obtained from **1–10** resulting in the comparative chemical structure-hydrogen bonding mode study presented herein. It should not be assumed that the X-ray structures presented here accurately predict solution state behaviour as solvent and packing effects amongst others may alter the self-associative mode observed in either state. However, this study does provide an insight into the fundamental self-associative modes that this class of compound are capable of adopting and the forces that may affect the presence of one binding mode over another. In Details for the synthesis of these single crystals are given in the ESI.†

Experimental

The synthesis of **3**, **4** and **8** have been previously reported.[10] Compounds **1** and **2** were synthesised by the reaction of aminomethanesulfonic acid (AMS) with the appropriate isocyanate and tetrabutylammonium (TBA) hydroxide in methanol. After further purification the pure products were obtained as white solids in yields of 33% and 18% respectively. Compounds **5**, **6** and **7** were synthesised by the reaction of AMS with the appropriate isocyanate or isothiocyanate in pyridine, followed by the addition of TBA hydroxide to produce the TBA salt. After further purification the pure products were obtained as white solids in yields of 52%, 19% and 63% respectively. Compound **10** was obtained through the reaction of the appropriate isocyanate with AMS in pyridine to give a white solid with a yield of 82%. Compound **9** was synthesised from compound **10** through the addition of sodium hydroxide in water, giving the pure product as colourless crystals in a quantitative yield. Full synthesis details for **1–10** are given in the ESI.†

In general, a suitable crystal of each compound was selected and mounted on a Rigaku Oxford Diffraction Supernova diffractometer. Data were collected using Cu Kα radiation to a maximum resolution of 0.84 Å. Each crystal was kept at 100(1) K during data collection, with the exception of compound **1**, which was collected at 300 K due to crystal shattering on cooling below room temperature. In all cases the crystal temperature was controlled using an Oxford Cryosystems 800-series Cryostream. The structure was solved with the ShelXT[16] structure solution program using Direct Methods and refined with ShelXL[17] on Least Squares minimisation. Olex2[18] was used as an interface to all ShelX programs.

Several of these compounds were crystalised as water solvates as discussed in the text and detailed in Table 2. The crystal structure of **5** also includes half a DMSO molecule per anion/cation pair. There is minor to moderate disorder observed in the TBA moieties of several structures (compounds **1**, **3b**, **4**, **5**, **6** and **7**). This is common for compounds with long alkyl chains and was modelled using a combination of restraints and constraints as appropriate to ensure a stable and chemically sensible model. There is also some minor disorder in the sulfonate-urea moieties in compounds **1** and **7**, and the DMSO in compound **5**, all of which were modelled in a similar fashion. Full refinement details can be found in the associated cifs.‡

Self-associative hydrogen bonding modes

Compounds **1–7** all contain the weakly coordinating TBA cation.[19] The modification of $R_1/R_2/X$ substituents within this series changes the NH HBD acidity, with a general increase from **1** to **7**. This is due to the electron donating or withdrawing nature of the R groups and the negative charge stabilisation effects of thiourea as opposed to the urea functionalities. The relative increase in HBD acidity promotes the formation of increasingly stable hydrogen bonds. The eight single crystal X-ray structures obtained from samples of **1–7** all showed the formation of intermolecular urea–anion

‡ X-ray data were collected on a SuperNova, Dual, Cu at zero, AtlasS2 diffractometer. CCDC numbers for the 11 single crystal structures from compounds **1–10**: **1** = 1489604; **2** = 1489605; **3a** = 1489606; **3b** = 1453959; **4** = 1489607; **5** = 1489608; **6** = 1489609; **7** = 1489610; **8** = 1453958; **9** = 1489611; **10** = 1489612.

Table 2 Single crystal X-ray structure information

Compound	1	2	3b	4	5	6	7	9	10
Empirical formula	$C_{25}H_{47}N_3O_5S$	$C_{24}H_{47}N_3O_5S$	$C_{24}H_{45}N_4O_{7.5}S$	$C_{25}H_{45}F_3N_3O_{4.5}S$	$C_{26}H_{48}F_3N_3O_4S_{2.5}$	$C_{26}H_{43}F_6N_3O_4S$	$C_{26}H_{43}F_6N_3O_4S_2$	$C_9H_{10}F_3N_2NaO_5S$	$C_{14}H_{14}F_3N_3O_4S$
Formula weight	501.72	489.70	525.70	548.70	603.82	607.51	639.75	338.24	377.34
Temperature/K	300(1)	100(1)	100(1)	100(1)	100(1)	100(1)	100(1)	100(1)	100(1)
Crystal system	Triclinic	Orthorhombic	Monoclinic	Monoclinic	Triclinic	Monoclinic	Triclinic	Orthorhombic	Triclinic
Space group	$P\bar{1}$	$Pna2_1$	$C2/c$	$C2/c$	$P\bar{1}$	$P2_1/n$	$P\bar{1}$	$P2_12_12_1$	$P\bar{1}$
a/Å	10.8520(3)	9.33311(13)	19.1853(5)	19.4863(8)	12.3465(7)	13.3272(4)	12.1225(5)	4.8741(3)	9.1526(3)
b/Å	14.2506(6)	18.8139(3)	16.9662(4)	16.9500(6)	13.2148(9)	20.7771(6)	13.1483(4)	6.3672(4)	12.9487(5)
c/Å	19.6911(8)	15.7107(2)	19.0342(5)	19.0704(5)	20.8662(10)	22.3152(6)	21.4144(11)	40.456(3)	13.3592(6)
α/°	96.202(3)				78.866(5)		74.424(4)		93.444(4)
β/°	103.112(3)		109.850(3)	110.145(4)	76.851(4)	92.086(3)	87.100(4)		97.949(3)
γ/°	94.223(3)				82.631(5)		84.476(3)		92.527(3)
Volume/Å^3	2933.22(19)	2758.68(7)	5827.5(3)	5913.5(4)	3240.1(3)	6175.0(3)	3271.5(2)	1255.54(14)	1563.01(11)
Z	4	4	4	8	2	4	4	4	4
ρ_{calc} g cm^{-3}	1.136	1.179	1.198	1.233	1.238	1.307	1.299	1.789	1.604
Crystal size/mm^3	0.274 × 0.117 × 0.033	0.372 × 0.06 × 0.047	0.507 × 0.18 × 0.094	0.212 × 0.083 × 0.067	0.136 × 0.05 × 0.017	0.335 × 0.07 × 0.026	0.28 × 0.106 × 0.004	0.596 × 0.103 × 0.087	0.324 × 0.181 × 0.132
Radiation	CuKα (λ = 1.54184)	CuKα (λ = 1.54184)	CuKα (λ = 1.54184)	CuKα (λ = 1.54184)	CuKα (λ = 1.54184)	CuKα (λ = 1.54184)	CuKα (λ = 1.54184)	CuKα (λ = 1.54184)	CuKα (λ = 1.54184)
2Θ range for data collection/°	4.646 to 133.184	7.33 to 146.048	7.152 to 146.196	7.11 to 133.2	4.412 to 133.198	5.814 to 146.124	7.006 to 133.2	4.368 to 145.696	6.696 to 145.966
Index ranges	$-8 \le h \le 12$, $-16 \le k \le 15$, $-23 \le l \le 23$	$-11 \le h \le 6$, $-22 \le k \le 20$, $-13 \le l \le 19$	$-23 \le h \le 19$, $-14 \le k \le 20$, $-23 \le l \le 22$	$-18 \le h \le 23$, $-14 \le k \le 20$, $-20 \le l \le 22$	$-10 \le h \le 14$, $-14 \le k \le 15$, $-20 \le l \le 24$	$-16 \le h \le 15$, $-25 \le k \le 25$, $-27 \le l \le 26$	$-14 \le h \le 14$, $-12 \le k \le 15$, $-24 \le l \le 25$	$-5 \le h \le 4$, $-7 \le k \le 7$, $-49 \le l \le 47$	$-7 \le h \le 11$, $-14 \le k \le 16$, $-16 \le l \le 15$
Reflections collected	20 872	6432	11 139	9536	21 922	25 495	21 742	7871	10 664
Independent reflections	11 353 R_{int} = 0.0179 R_{sigma} = 0.0261	3810 R_{int} = 0.0241 R_{sigma} = 0.0365	5674 R_{int} = 0.0305 R_{sigma} = 0.0315	5202 R_{int} = 0.0146 R_{sigma} = 0.0200	11 448 R_{int} = 0.0564 R_{sigma} = 0.0942	12 024 R_{int} = 0.0386 R_{sigma} = 0.0479	11 568 R_{int} = 0.0335 R_{sigma} = 0.0475	2439 R_{int} = 0.0288 R_{sigma} = 0.0262	6036 R_{int} = 0.0229 R_{sigma} = 0.0283
Data/restraints/parameters	11 353/549/724	3810/1/309	5674/176/381	5202/926/486	11 448/36/717	12 024/45/748	11 568/898/896	2439/0/192	6036/0/455
GOOF on F^2	1.031	1.031	1.034	1.045	1.034	1.017	1.055	1.066	1.128
Final R indexes [$I \ge 2\sigma(I)$]	R_1 = 0.0564 wR_2 = 0.1675	R_1 = 0.0300 wR_2 = 0.0750	R_1 = 0.0794 wR_2 = 0.2289	R_1 = 0.0602 wR_2 = 0.1485	R_1 = 0.0543 wR_2 = 0.1208	R_1 = 0.0447 wR_2 = 0.1058	R_1 = 0.1110 wR_2 = 0.3006	R_1 = 0.0279 wR_2 = 0.0697	R_1 = 0.0424 wR_2 = 0.1103
Final R indexes [all data]	R_1 = 0.0789 wR_2 = 0.1933	R_1 = 0.0316 wR_2 = 0.0764	R_1 = 0.0860 wR_2 = 0.2406	R_1 = 0.0690 wR_2 = 0.1558	R_1 = 0.0819 wR_2 = 0.1386	R_1 = 0.0581 wR_2 = 0.1152	R_1 = 0.1342 wR_2 = 0.3293	R_1 = 0.0288 wR_2 = 0.0701	R_1 = 0.0441 wR_2 = 0.1113
Largest diff. peak/hole/e Å^{-3}	0.39/−0.22	0.35/−0.31	0.51/−0.63	0.50/−0.47	0.49/−0.69	0.30/−0.41	1.77/−0.95	0.31/−0.40	0.45/−0.55
Flack parameter		0.033(16)						0.34(2)	

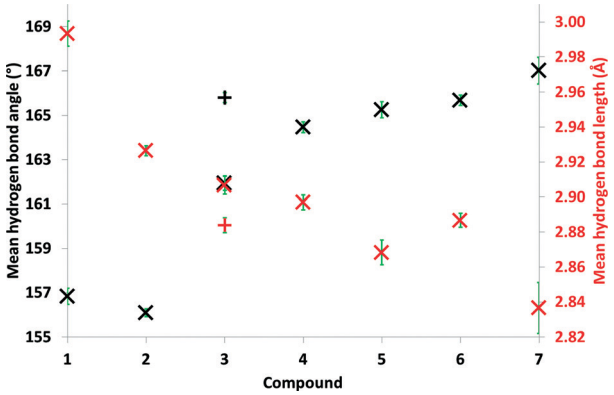

Fig. 2 Mean hydrogen bond angles (°) and lengths (Å) responsible for the anion–urea binding modes in each of the eight different crystal structures obtained from compounds **1**, **2**, **3** (+ = **3a**; X = **3b**), **4**, **5**, **6**, **7**. Table S1† details individual hydrogen bond lengths, angles and associated errors observed in each single crystal X-ray structure.

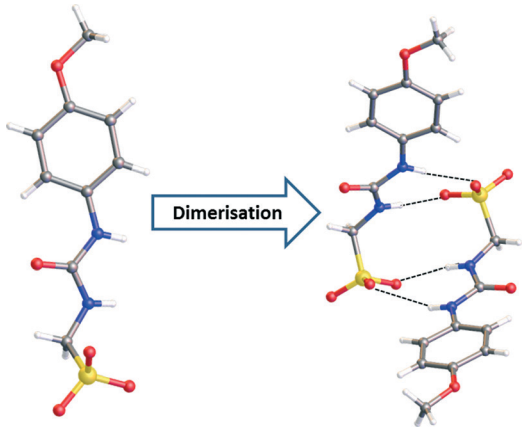

Fig. 4 Ball and stick representation of the hydrogen bonded dimer formed with **1**. In this instance the minor component of disorder has been omitted for clarity. Atomic colour scheme: carbon = grey; oxygen = red; nitrogen = blue; sulfur = yellow; hydrogen = white.

binding modes. Two different crystal structures were obtained for **3**, one of which is a solvate (**3a**) and the other is solvent free (**3b**). Mean hydrogen bond lengths and angles were calculated for those hydrogen bonds contributing directly to urea–anion self-associative complex formation. As shown in Fig. 2, the mean hydrogen bond angle was found to increase towards the optimal 180° and mean hydrogen bond length found to decrease as HBD acidity was increased from **1**–**7**, indicating the formation of increasingly stable hydrogen bonds. A similar trend, shown in Fig. 3, was also identified when comparing the mean hydrogen bond lengths and angles of the structurally similar urea based compounds **1**–**4** and **6** with the corresponding Hammett substituent constants (σ) based on the ionisation of benzoic acids.[20]

As shown in Fig. 4 and 5, structures obtained from **1**, **3**–**7** all exhibit urea–anion dimer formation through the creation of four intermolecular hydrogen bonds, one from each HBD NH to a separate HBA oxygen of an anionic sulfonate group. Conversely **2**, (Fig. 6) was found to form urea–anion hydrogen bonded tapes. Unlike the hydrogen bonded dimers, both the HBD NHs of a single urea group coordinate to a single HBA oxygen of a sulfonate functionality.

Single crystal X-ray structures for **2**, **3a**, **4** and **7** all show the additional coordination of a water molecule to the anionic sulfonate substituent, through additional hydrogen

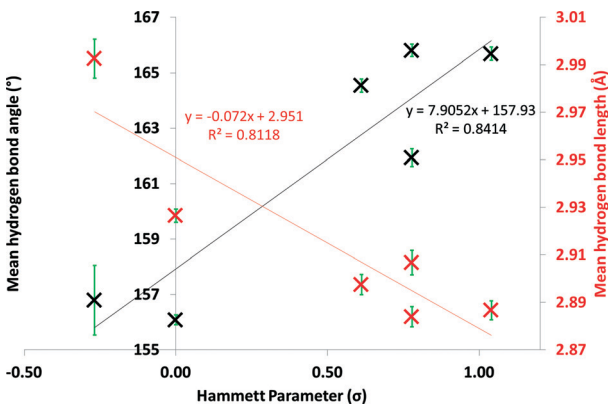

Fig. 3 Correlation between Hammett substituent constants[20] (σ) and mean hydrogen bond angles (°) or lengths (Å) responsible for the anion–urea binding modes in each of the six different crystal structures obtained for comparable compounds **1**, **2**, **3** (**3a**; **3b**), **4**, **6**.

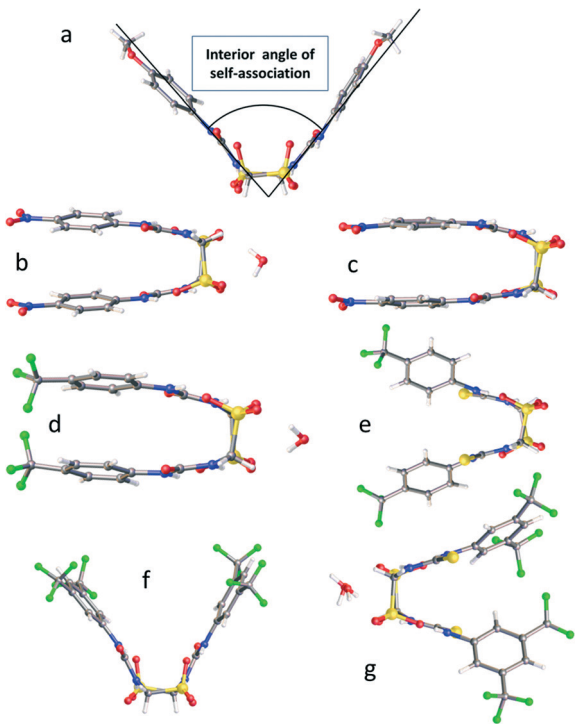

Fig. 5 Ball and stick representation of the single crystal X-ray structures obtained for compounds **1**, **3**–**7**, exhibiting hydrogen bonded dimerisation through a urea–anion binding mode. TBA counter ions, DMSO solvent molecules and minor components of disorder have been omitted for clarity; a) **1**; b) **3a**; c) **3b**; d) **4**; e) **5**; f) **6**; g) **7**. Atomic colour scheme: carbon = grey; oxygen = red; nitrogen = blue; sulfur = yellow; hydrogen = white; fluorine = green.

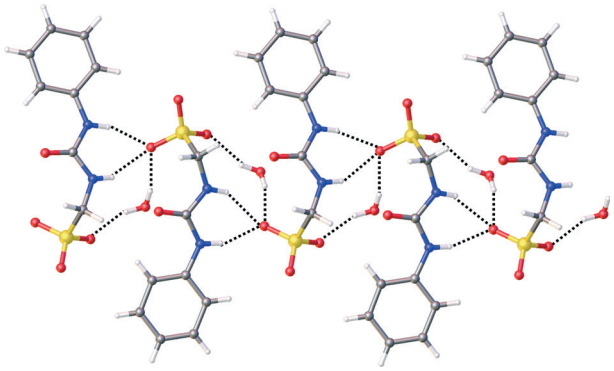

Fig. 6 Ball and stick representation of the single crystal X-ray structure obtained for compound **2**, exhibiting hydrogen bonded tape formation through a urea–anion binding mode. TBA counter ions have been omitted for clarity. Atomic colour scheme: carbon = grey; oxygen = red; nitrogen = blue; sulfur = yellow; hydrogen = white.

bonds. The two comparative structures obtained for **3** (**3a** – Fig. 5b, **3b** – Fig. 5c) suggest that in this instance the additional coordination of water to the sulfonate-urea dimer contributes to the increased stability of the hydrogen bonded complex. This is evidenced by the reduction in hydrogen bond lengths and optimisation of hydrogen bond angles, shown in Fig. 2.

To further compare the self-associative binding modes observed with **1**–**7**, the interior angle of the hydrogen bonded dimers and tapes was calculated from the intercepting planes of the urea/thiourea substituents, as illustrated in Fig. 5a. This angle is smallest for the dimers formed from **3** with angles of 21.20(17)° and 19.90(12)° calculated for **3a** and **3b** respectively. Exchanging the urea functionality for a thiourea with compounds **4** and **5** resulted in a slight increase in interior bond angle from 22.60(18)° to 29.77(10)° respectively. The increase in steric bulk with the addition of multiple CF_3

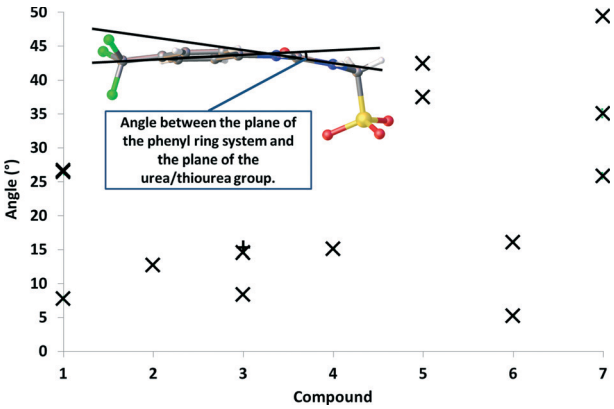

Fig. 7 Estimation of anion twist obtained though calculating the angle between the planes of the covalently linked phenyl ring system and urea/thiourea substituent of each individual anionic component contained in the crystal structures of **1**–**7** (+ = **3a**; X = **3b**). This also includes different disordered components where appropriate. Atomic colour scheme: carbon = grey; oxygen = red; nitrogen = blue; sulfur = yellow; hydrogen = white; fluorine = green. Errors ≤ ±0.6°.

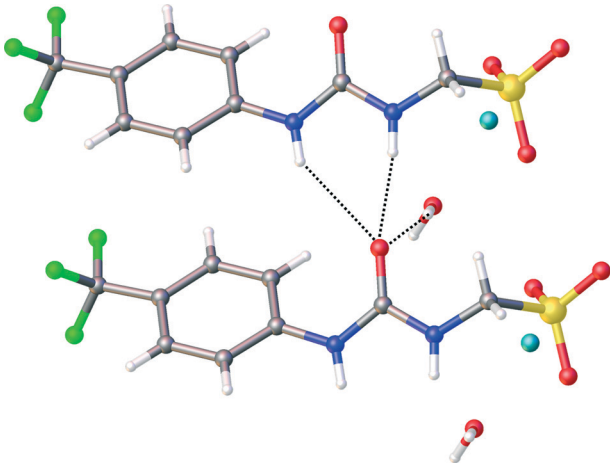

Fig. 8 Ball and stick representation of the single crystal X-ray structure obtained for compound **9**, exhibiting hydrogen bonded tape formation through a *syn*-urea–urea binding mode. Table S1† details individual hydrogen bond lengths, angles and associated errors observed in this single crystal X-ray structure. Atomic colour scheme: carbon = grey; oxygen = red; nitrogen = blue; sulfur = yellow; hydrogen = white; fluorine = green; sodium = turquoise.

functionalities for **6** and **7** was also found to increase the interior angle to 53.45(8)° and 32.6(2)° respectively. However, in this instance the interior self-association angle is greater for the urea compared to the thiourea. Compound **2**, which was found to adopt the tape conformation, was also found to have the largest interior angle of 160.68(15)° with compound **1**, which contains the least acidic HBD groups also exhibiting a large interior angle of 73.61(12)°. The angle between the plane of the phenyl ring and urea/thiourea groups were also compared as shown in Fig. 7. The structures which contain the urea HBD group were found to exhibit approximately planar monomeric structures, where as those containing the thiourea functionality were found to exhibit a greater twist.

Replacing the TBA counter cation of **4** with potassium and sodium, gives **8** and **9** respectively. Neither **8** nor **9** exhibit self-associative urea–anion binding modes, but instead show *syn*-urea–urea binding modes, as illustrated in Fig. 8. Both the sodium and potassium cations are known to strongly coordinate anions in comparison to TBA.[19] This explains the switch from the urea–anion binding mode of **4** to the urea–urea binding mode observed with **8** and **9**. The sulfonate group is no longer free to act as a HBA, the urea oxygen atom has now become the principle HBA in the self-association process.

Exchanging the strongly sulfonate coordinating sodium/potassium counter cation of **8** and **9** for the less strongly sulfonate coordinating HBD pyridinium ion gives rise to **10**. The counter cation acts as a competitive HBD, coordinating to the HBA sulfonate functionalities as shown in Fig. 9a. In this instance we no longer see the formation of the self-associative urea–urea binding mode as with **8** and **9** or the urea–anion dimer formation as with **4**. Instead **10** adopts a similar urea–anion hydrogen bonded tape to **2**, illustrated in Fig. 9b. The

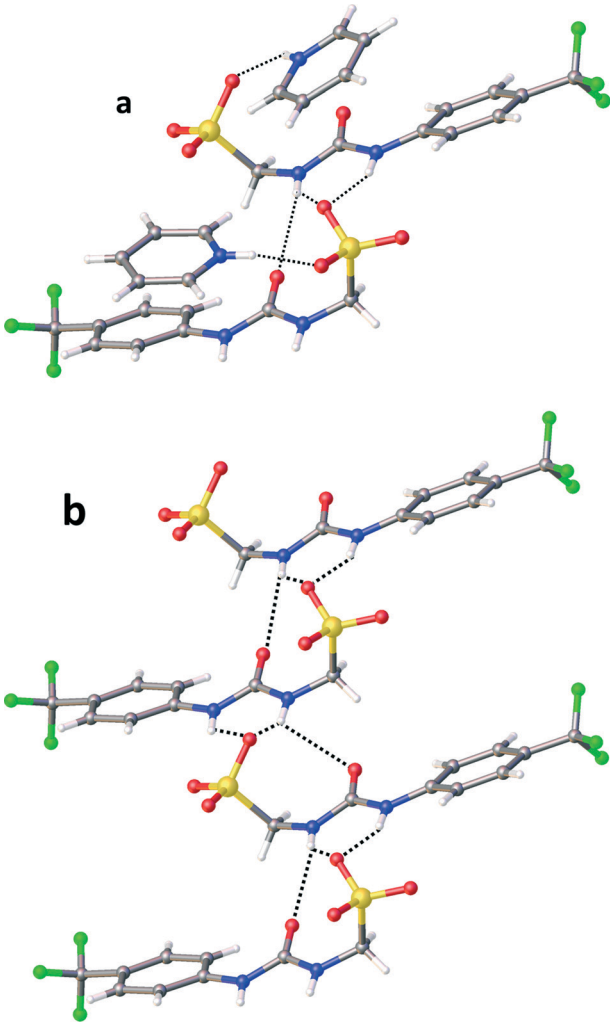

Fig. 9 Ball and stick representation of the single crystal X-ray structure obtained for compound **10**, exhibiting hydrogen bonded tape formation through a urea–anion binding mode; a) showing the hydrogen bonding modes produced through the additional HBD capabilities of the pyridinium counter cation; b) shows the extended hydrogen bonded tape. Table S1† details individual hydrogen bond lengths, angles and associated errors observed in this single crystal X-ray structure. Atomic colour scheme: carbon = grey; oxygen = red; nitrogen = blue; sulfur = yellow; hydrogen = white; fluorine = green.

mean intermolecular urea–anion hydrogen bond calculated for **10** measured 154.60(29)° and 2.967(4) Å. Compound **4** was shown to have a comparative mean bond angle of 164.47(24)° and mean hydrogen bond length of 2.897(4) Å, suggesting the anion–urea hydrogen bonds formed in the self-association of **10** are comparatively weaker to those of **4**. This can be attributed to the cation exchange.

Extended architectures

Taking an expanded view of the molecular architectures produced by this family of 'frustrated' amphiphilic salt in the solid state shows the formation of structures which resemble

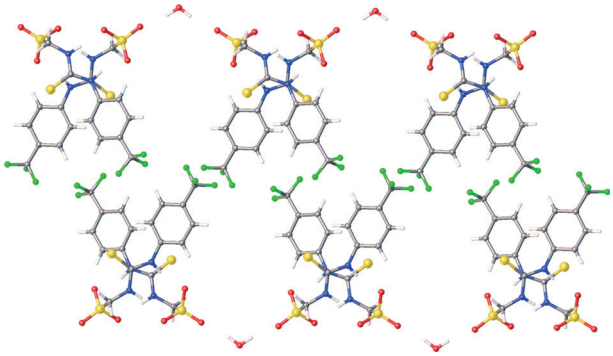

Fig. 10 Ball and stick representation of the expanded molecular architecture of compound **5**, to produce two dimensional tapes. Atomic colour scheme: carbon = grey; oxygen = red; nitrogen = blue; sulfur = yellow; hydrogen = white; fluorine = green.

biological bilayers and hydrophilic water channels. There is no evidence to suggest that these structures are maintained within the solution state however, work in this area is ongoing. Over billions of years cells have evolved to become incredibly complex miniaturized factories, each containing thousands of pieces of complex molecular machinery with a specific purpose, remaining unparalleled by any synthetic systems.[21] In recent times there has been an explosion of interest in synthetic biologically inspired systems. This includes the synthesis of artificial channels[22] for the selective transport of ions[23] and polar molecules, such as water[24–31] across phospholipid bilayers as illustrated by Davis *et al.*[32] and Percec *et al.*;[33,34] the synthesis of biologically inspired molecular machines as illustrated by Leigh *et al.*;[35–37] and

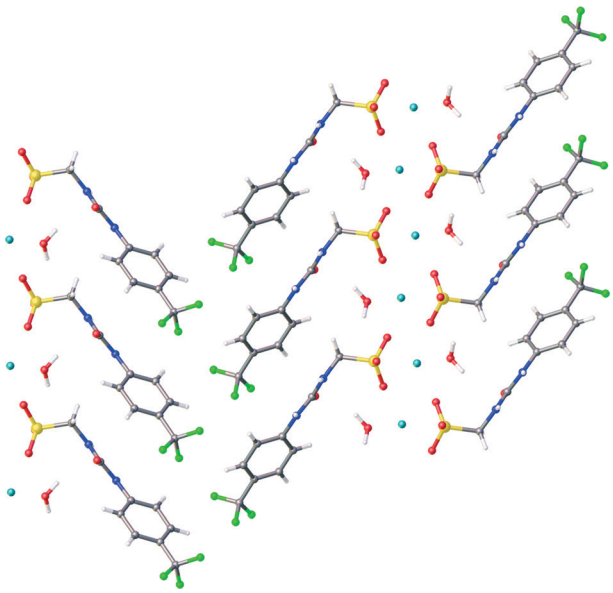

Fig. 11 Ball and stick representation of the expanded molecular architecture of compound **9**. Atomic colour scheme: carbon = grey; oxygen = red; nitrogen = blue; sulfur = yellow; hydrogen = white; fluorine = green; sodium = turquoise.

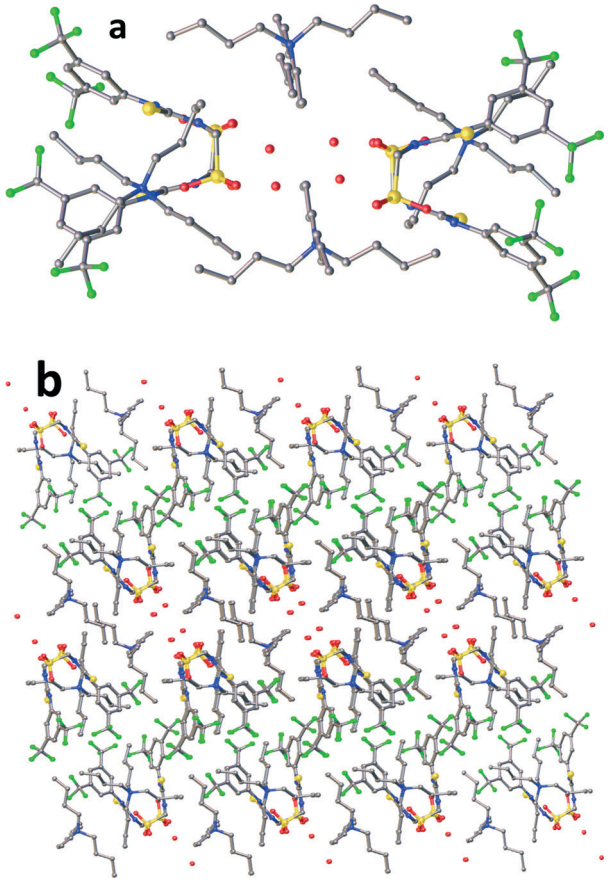

Fig. 12 Ball and stick representation of the a) pseudo water channel formation, hydrogen atoms and minor components of disorder have been omitted for clarity; b) expanded molecular architecture of compound **7**. Atomic colour scheme: carbon = grey; oxygen = red; nitrogen = blue; sulfur = yellow; fluorine = green.

the development or utilisation of synthetic biologically inspired membranes.[38–41]

Bilayer-like structures

The hydrogen bonded urea–anion dimers formed by **5** were found to undergo further self-assembly processes to produce two dimensional hydrogen bonded tapes, as shown in Fig. 10. The hydrophobic interior consists of the CF_3 substituted aromatic groups. The peripheral edges of these tapes consist of hydrophilic sulfonate functionalities with hydrogen bonded water molecules acting as a bridge between the urea–anion hydrogen bonded dimers.

Fig. 11 shows that **9**, adopts a similar expanded architecture to that exhibited in by compound **5**, through the formation of linear hydrophobic and hydrophilic zones. The hydrophobic zones again consist of the CF_3 substituted aromatic groups. The hydrophilic zones comprise of the sulfonate functionalities, sodium cations and water molecules. In this instance the presence of the urea–urea binding mode cause these hydrogen bonded tapes to running anti-parallel to one another. An analogous molecular architecture was also observed within the crystal structure of **8**.

Water channel-like structures

The urea–anion hydrogen bonded dimers of **7** are observed to form pseudo water channels as illustrated in Fig. 12a. Water molecules permeate through this crystal structure coordinated, through the formation of hydrogen bonds, to the sulfonate functionalities which provide a hydrophilic surface to the internal cavity of these pseudo water channels. The TBA and aromatic CF_3 functionalities surround these hydrophilic cores enclosing them in a hydrophobic barrier. Fig. 12b illustrates how these pseudo water channels pack together in the expanded molecular architecture.

Conclusions

As previously discussed, clearly identifying the different self-associative non-covalent binding modes adopted by this class of 'frustrated' amphiphile in the solution state is technically challenging. The analysis of eleven single crystal X-ray structures obtained from a library of ten analogous amphiphilic salts have illustrated how different types of binding mode may be achieved through the modulation of the amphiphiles different functionalities. We have shown that within the solid state the presence of a weakly coordinating counter cation such as TBA results primarily in the formation of urea–anion dimers. Modulating the HBD acidity through replacement of the R and X groups was found to alter the length and angle of the hydrogen bonds formed within the complex, which in turn affects the interior angle of the dimers formed. The more acidic the HBD groups, the more optimal the formation of the urea–anion hydrogen bond. The replacement of the TBA with a pyridinium cation that is able to act as a competitive HBD results in a switch from urea–anion dimer to the urea–anion tape, decreasing optimal urea–anion hydrogen bond formation. Exchange of weakly sulfonate coordinating cations such as TBA or pyridinium with strongly sulfonate coordinating potassium/sodium counter cations prevents the formation of the urea–anion binding mode, giving rise to the urea–urea binding mode. Comparative investigations into the self-association of these amphiphilic salts within the solution state are currently ongoing.

Acknowledgements

JRH would like to thank the University of Kent for the Caldin Fellowship, K. Howland (mass spectrometry), G. P. Bustone (summer student) and B. Wilson (summer student). JRH would also like to thank M. Sambrook for the years of mentorship he has given.

Notes and references

1 C. Wang, Z. Wang and X. Zhang, *Acc. Chem. Res.*, 2012, **45**, 608–618.
2 G. Yu, K. Jie and F. Huang, *Chem. Rev.*, 2015, **115**, 7240–7303.

3 S. Kumar, K. Ludwig, B. Schade, H. von Berlepsch, I. Papp, R. Tyagi, M. Gulia, R. Haag and C. Boettcher, *Chem. – Eur. J.*, 2016, **22**, 5629–5636.
4 B. N. S. Thota, L. H. Urner and R. Haag, *Chem. Rev.*, 2016, **116**, 2079–2102.
5 J. Wang, X. Wang, F. Yang, H. Shen, Y. You and D. Wu, *Langmuir*, 2015, **31**, 13834–13841.
6 G. Yu, K. Jie and F. Huang, *Chem. Rev.*, 2015, **115**, 8944.
7 X. D. Xu, X. Li, H. Chen, Q. Qu, L. Zhao, H. Ågren and Y. Zhao, *Small*, 2015, **11**, 5901–5906.
8 C. Aime, R. Tamoto, T. Satoh, A. Grelard, E. J. Dufourc, T. Buffeteau, H. Ihara and R. Oda, *Langmuir*, 2009, **25**, 8489–8496.
9 M. Ma, A. Paredes and D. Bong, *J. Am. Chem. Soc.*, 2008, **130**, 14456–14458.
10 J. R. Hiscock, G. P. Bustone, B. Wilson, K. E. Belsey and L. R. Blackholly, *Soft Matter*, 2016, **12**, 4221–4228.
11 C. M. C. Faustino, A. R. T. Calado and L. Garcia-Rio, *J. Colloid Interface Sci.*, 2012, **367**, 286–292.
12 C. M. C. Faustino, A. R. T. Calado and L. Garcia-Rio, *Biomacromolecules*, 2009, **10**, 2508–2514.
13 C. M. C. Faustino, A. R. T. Calado and L. Garcia-Rio, *J. Phys. Chem. B*, 2009, **113**, 977–982.
14 C. M. C. Faustino, A. R. T. Calado and L. Garcia-Rio, *J. Colloid Interface Sci.*, 2011, **359**, 493–498.
15 C. M. C. Faustino, A. R. T. Calado and L. Garcia-Rio, *J. Colloid Interface Sci.*, 2010, **351**, 472–477.
16 G. M. Sheldrick, *Acta Crystallogr., Sect. A: Found. Adv.*, 2015, **71**, 3–8.
17 G. M. Sheldrick, *Acta Crystallogr., Sect. C: Struct. Chem.*, 2015, **71**, 3–8.
18 O. V. Dolomanov, L. J. Bourhis, R. J. Gildea, J. A. K. Howard and H. Puschmann, *J. Appl. Crystallogr.*, 2009, **42**, 339–341.
19 R. Shukla, T. Kida and B. D. Smith, *Org. Lett.*, 2000, **2**, 3099–3102.
20 D. H. McDaniel and H. C. Brown, *J. Org. Chem.*, 1958, **23**, 420–427.
21 M. Denton, *Evolution: A Theory in Crisis*, Adler & Adler, 1986.
22 W. Si, P. Xin, Z.-T. Li and J.-L. Hou, *Acc. Chem. Res.*, 2015, **48**, 1612–1619.
23 G. W. Gokel and S. Negin, *Acc. Chem. Res.*, 2013, **46**, 2824–2833.
24 M. Barboiu, *Angew. Chem., Int. Ed.*, 2012, **51**, 11674–11676.
25 M. Barboiu, *Chem. Commun.*, 2016, **52**, 5657–5665.
26 M. Barboiu, P.-A. Cazade, Y. L. Duc, Y.-M. Legrand, A. van der Lee and B. Coasne, *J. Phys. Chem. B*, 2015, **119**, 8707–8717.
27 M. Barboiu and A. Gilles, *Acc. Chem. Res.*, 2013, **46**, 2814–2823.
28 M. Barboiu, Y. Le Duc, A. Gilles, P.-A. Cazade, M. Michau, Y. M. Legrand, A. van der Lee, B. Coasne, P. Parvizi, J. Post and T. Fyles, *Nat. Commun.*, 2014, **5**, 1–8.
29 Y. Le Duc, M. Michau, A. Gilles, V. Gence, Y. M. Legrand, A. van der Lee, S. Tingry and M. Barboiu, *Angew. Chem., Int. Ed.*, 2011, **50**, 11366–11372.
30 Y. M. Legrand, M. Michau, A. van der Lee and M. Barboiu, *CrystEngComm*, 2008, **10**, 490–492.
31 Y. M. Legrand, A. van der Lee, N. Masquelez, P. Rabu and M. Barboiu, *Inorg. Chem.*, 2007, **46**, 9083–9089.
32 M. S. Kaucher, W. A. Harrell and J. T. Davis, *J. Am. Chem. Soc.*, 2006, **128**, 38–39.
33 M. S. Kaucher, M. Peterca, A. E. Dulcey, A. J. Kim, S. A. Vinogradov, D. A. Hammer, P. A. Heiney and V. Percec, *J. Am. Chem. Soc.*, 2007, **129**, 11698–11699.
34 V. Percec, A. E. Dulcey, V. S. K. Balagurusamy, Y. Miura, J. Smidrkal, M. Peterca, S. Nummelin, U. Edlund, S. D. Hudson, P. A. Heiney, D. A. Hu, S. N. Magonov and S. A. Vinogradov, *Nature*, 2004, **430**, 764–768.
35 S. Erbas-Cakmak, D. A. Leigh, C. T. McTernan and A. L. Nussbaumer, *Chem. Rev.*, 2015, **115**, 10081–10206.
36 E. R. Kay and D. A. Leigh, *Angew. Chem., Int. Ed.*, 2015, **54**, 10080–10088.
37 B. Lewandowski, G. De Bo, J. W. Ward, M. Papmeyer, S. Kuschel, M. J. Aldegunde, P. M. E. Gramlich, D. Heckmann, S. M. Goldup, D. M. D'Souza, A. E. Fernandes and D. A. Leigh, *Science*, 2013, **339**, 189–193.
38 Y. K. Lee, H. Lee and J.-M. Nam, *NPG Asia Mater.*, 2013, **5**, 1–13.
39 S. Rao, K. J. Si, L. W. Yap, Y. Xiang and W. Cheng, *ACS Nano*, 2015, **9**, 11218–11224.
40 A. Janshoff and C. Steinem, *Anal. Bioanal. Chem.*, 2006, **385**, 433–451.
41 T. Kunitake, *Angew. Chem., Int. Ed. Engl.*, 1992, **31**, 709–726.

